

ArH₂⁺ and NeH₂⁺ as Global Minima in the Ar⁺/Ne⁺ + H₂ Reactions: Energetic, Spectroscopic, and Structural Data

Riley A. Theis, W. James Morgan, and Ryan C. Fortenberry*

Georgia Southern University, Department of Chemistry, Statesboro, GA 30460 U.S.A.

Submitted: 31 July 2021

Key words: astrochemistry – molecular data – molecular processes – ISM: molecules – radio lines: ISM – infrared: ISM

ABSTRACT

In light of the recent discovery of ArH⁺ in the Crab nebula, it is shown through high-level quantum chemical computations that the global minima on the Ar⁺/Ne⁺ + H₂ potential energy surfaces are ArH₂⁺ and NeH₂⁺. Hence, ArH₂⁺ may be a necessary intermediate in the Ar⁺ + H₂ → ArH⁺ + H formation reaction proposed in the same work where ArH⁺ is first reported in the Crab nebula. ArH₂⁺ is also probably an intermediate in the alternative Ar + H₂⁺ → ArH⁺ + H reaction. Additionally, it is shown that Ne⁺ + H₂ → NeH₂⁺ will subsequently most likely yield Ne + H₂⁺ and not NeH⁺ + H offering a possible rationale as to the absence of NeH⁺ in spectra obtained from the interstellar medium (ISM). Following from this, spectroscopic data (both rotational and vibrational) are provided for NeH₂⁺ and ArH₂⁺ through the use of highly-accurate quantum chemical quartic and cubic force fields. All possible isotopologues are also included for ²⁰Ne, ²²Ne, ³⁶Ar, ³⁸Ar, ⁴⁰Ar, ¹H, and D. The dipole moments for these systems are quite large at 5.61 D for NeH₂⁺ and 4.37 D for ArH₂⁺. The spectroscopic constants provided will aid in the potential detection of these open-shell noble gas dihydride cations in the ISM.

1 INTRODUCTION

The recent detection of the noble gas compound ³⁶ArH⁺ in the Crab nebula (Barlow et al. 2013) and, more recently in various other regions (Schilke et al. 2014), has tremendously opened up the chemistry of the interstellar medium (ISM), and has led to questions about the provenance of this molecule (Roueff et al. 2014) and the possible existence of other noble gas compounds to be found in various regions of the ISM. ArH⁺ has been proposed to form via the Ar⁺ + H₂ reaction in the ISM (Barlow et al. 2013) and has been explored both observationally and theoretically (Schilke et al. 2014; Roueff et al. 2014). The noble gases (He, Ne, Ar, Kr, Xe) have been called “noble” due to their aversion to chemical reactivity brought about by the complete filling of their valence electron shell. Hence, electrons are not easily shared by these atoms and bonds are not typically made. However, noble gas atoms can be polarized by various substituent groups, and cationic and van der Waals noble gas compounds have long been studied (Grandinetti 2011). What is intriguing and ground-breaking about the discovery of ArH⁺ in the Crab nebula is that a noble gas compound has finally been shown to exist somewhere in nature.

The ISM is a natural place to find noble gas compounds where the pressures and temperatures of a given region may be just right for the synthesis of terrestrially unstable molecules. Radicals and even anions have been commonly detected in the ISM by comparison, largely, to spectroscopic data made available in databases like the Cologne Database for Molecular Spectroscopy (CDMS) (Müller et al. 2005). However, the chief problem with the detection of noble gas compounds in the ISM is a lack of adequate spectroscopic data since these molecules are difficult to study in the laboratory combined with the ensuing fact that little need has previously been demonstrated for such data. A follow-up study (Cueto et al. 2014) to this initial discovery has produced highly-accurate rovibrational reference data for ³⁶ArH⁺, as well as the other abundant Ar isotope ³⁸ArH⁺, in order to augment that from the CDMS which was used in the detection of ³⁶ArH⁺ in the Crab nebula. Hence, if more noble gas compounds are to be detected, reliable spectroscopic data must be generated.

Searches for the related HeH⁺ and NeH⁺ are almost certainly underway if not already completed (Schilke et al. 2014). It is unlikely that noble gas compounds containing krypton and xenon will be observed since these atoms are both larger than iron and exist in substantially smaller abun-

dances. However, the large dipole moments exhibited by noble gas hydride cations (Cueto et al. 2014) brought about from the drastic difference between the centre-of-mass (very close to the noble gas atomic centre) and the centre-of-charge (roughly midway between the two atoms) make them very rotationally bright aiding in their potential detection as a class. Even so, other compounds containing He, Ne, and Ar are more likely to be observed in the ISM than those containing the heavier noble gas atoms.

Various noble gas species, both cationic and neutral, have been shown to be stable through laboratory experiments and quantum chemical computations. For example, high-resolution infrared data of the Ng-H₂ (Ng = Ne, Ar, Kr) structures have been provided (McKellar 1996, 2005, 2009), and computational studies as to their energy profiles, as well as that of HeH₂, have shown that these are minima on their respective potential energy surfaces (PESs) (Barletta 2009). Additionally, complexes of one to three noble gas atoms bonded to H₃⁺, a molecule of substantial importance to astrochemistry (Pavanello et al. 2012), have exhibited marked stabilities (Pauzat et al. 2009). Other noble gas molecules are known (Kim & Lee 1999; Borocci et al. 2011; Grandinetti 2011), but the next-simplest class of noble gas compounds are simply the Ng-H₂⁺ species.

There exists very little data on this class of compounds which is surprising due to their relative simplicity. Bartl et al. (2013) recently observed HeH₂⁺, in addition to “all conceivable combinations of n and x ” for He _{n} H _{x} ⁺, in mass spectrometry experiments, indicating that these Ng-H₂⁺ structures are likely stable minima, as well. Gamallo et al. (2013) studied the reaction of Ne + H₂⁺ and found that the global minimum on the PES is actually NeH₂⁺ following work on this same surface from Mayneris et al. (2008). Several studies have explored the interaction of argon atoms and atomic cations with hydrogen molecules and molecular cations (Bedford & Smith 1990; Tosi et al. 1993; Song & Gisalson 2003) where most of these build on the seminal work by Adams et al. (1970) where noble gas dimers were reacted with hydrogen molecules. ArH₂⁺ is believed to exist on the PES due to the relative energetics of the total surface, and it seems probable, therefore, that these Ng-H₂⁺ molecules are experimentally observable. However, spectroscopic data has not been provided for the Ng-H₂⁺ molecules in order to confirm their presence in these experiments.

In this present study, the formation/dissociation pathways of two Ng-H₂⁺ cations, NeH₂⁺ and ArH₂⁺, are provided. Additionally, the rovibrational spectroscopic data of these two noble gas dihydride cations are produced in order to assist in their potential discovery in the ISM. Building on previous quantum chemical studies that have generated rotational constants to better than 0.1% of the corresponding experimental values and fundamental vibrational frequencies within 5 cm⁻¹, or even 1 cm⁻¹ in some cases (Huang et al. 2011; Fortenberry et al. 2011a,b, 2012; Huang et al. 2013a), rotational constants, dipole moments, spectroscopic constants, and fundamental vibrational frequencies are provided for these two open-shell noble gas cations and their myriad isotopologues.

2 COMPUTATIONAL DETAILS

The highly-accurate structural and spectroscopic data necessary to examine the presence of NeH₂⁺ and ArH₂⁺ in any reaction scheme is derived here from quartic force fields (QFFs). QFFs are fourth-order Taylor series approximations to the nuclear Hamiltonian (Fortenberry et al. 2013) and are of the form:

$$V = \frac{1}{2} \sum_{ij} F_{ij} \Delta_i \Delta_j + \frac{1}{6} \sum_{ijk} F_{ijk} \Delta_i \Delta_j \Delta_k + \frac{1}{24} \sum_{ijkl} F_{ijkl} \Delta_i \Delta_j \Delta_k \Delta_l, \quad (1)$$

where Δ_i are displacements and $F_{ij\dots}$ are the force constants. These methods provide low-cost (relative to producing a global PES) but still high-accuracy computationally-derived spectroscopic data. The most accurate QFFs (Huang & Lee 2008, 2009; Huang et al. 2011) begin from coupled cluster singles, doubles, and perturbative triples [CCSD(T)] (Raghavachari et al. 1989) geometry optimizations with the cc-pV5Z basis sets (Dunning 1989; Peterson & Dunning 1995). Ar, however, requires the cc-pV(5+d)Z basis set (Peterson & Dunning 1995), but this will simply be called cc-pV5Z (and likewise for similar basis sets) for ease of discussion. The geometrical parameters are further corrected for the correlation of the core electrons by CCSD(T) geometry optimizations with the Martin-Taylor (MT) core-correlating basis set (Martin & Taylor 1994) derived to treat these properties. In this case, the difference between the CCSD(T)/MT bond lengths with core and those without core electrons are added to the CCSD(T)/cc-pV5Z bond lengths. All computations are based on restricted open-shell reference wavefunctions (Gauss et al. 1991; Lauderdale et al. 1991; Watts et al. 1993) for these open-shell cations.

From this linear reference geometry, a grid of 55 symmetry-unique points are used to define the QFF. Displacements of the two bond lengths are made in Δ_p increments of 0.005 Å, and the bond angle Δ_p increments are 0.005 radians. The Ng-H bond length is coordinate 1, the H-H bond length is coordinate 2, and the Ng-H-H bond angle is coordinate 3, where this latter term is treated in a linear-bending term defined in the INTDER program (Allen & coworkers 2005) and discussed elsewhere (Huang et al. 2011, 2013b). Degenerate with and perpendicular to coordinate 3 is the other Ng-H-H bond angle, which is designated as coordinate 4. However, the symmetry relationship of this coordinate to coordinate 3 negated explicit treatment of this angle (Huang & Lee 2009; Huang et al. 2013b). At each point, CCSD(T) energies are computed with the aug-cc-pVTZ, aug-cc-pVQZ, and aug-cc-pV5Z basis sets (Dunning 1989; Kendall et al. 1992), which are extrapolated to the one-particle complete basis set (CBS) limit via a three-point formula (Martin & Lee 1996). To these CBS energies, corrections for core correlation from the MT basis set with and without core electrons and scalar relativistic (Douglas & Kroll 1974) corrections are also made. This definition of the QFF is called the CcCR QFF from the “C” for CBS, “cC” for core correlation, and “R” for relativity (Fortenberry et al. 2011a).

The CcCR force constants are derived from a fitting of the QFF via a least-squares approach. This also produces the equilibrium geometry with a sum of squared residuals on the order of 10⁻¹⁹ a.u.² for NeH₂⁺ and 10⁻¹⁵ a.u.² for ArH₂⁺. Utilizing this new minimum, the force constants

are refit to produce zero gradients and positive quadratic terms along with subsequently more complete cubic and quartic terms. The force constants are then incorporated in the linear nuclear Hamiltonian via the SPECTRO program (Gaw et al. 1991), where second-order perturbation theory produces the spectroscopic constants (Mills 1972; Watson 1977) and vibrational frequencies (Papoušek & Aliev 1982). Most of the electronic structure computations make use of the PSI4 quantum chemistry package (Turney et al. 2012), but the scalar relativistic energy points as well as the CCSD(T)/aug-cc-pV5Z dipole moment computations utilize MOLPRO2012.1 (Werner et al. 2012) made available on the Pittsburgh Supercomputing Center’s Blacklight Cluster.

3 RESULTS AND DISCUSSION

3.1 NeH₂⁺ Structural and Spectroscopic Considerations

The force constants for ²Σ⁺ NeH₂⁺ are given in Table 1 following the coordinate ordering defined in the previous section. This linear structure is clearly a minimum since all of the second derivatives are positive, indicating an upward curve to the PES. The structural and spectroscopic data for ²⁰NeH₂⁺ and its deuterated isotopologues are given in Table 2 while the geometric and spectroscopic data for the less abundant neon isotopic cation, ²²NeH₂⁺, and its deuterated isotopologues are in Table 3. The force constants remain the same for any of the isotopologues since they are computed within the Born-Oppenheimer approximation. The NeH₂⁺ and NeHD⁺ molecules, regardless of neon isotope, require input of a $2\nu_2 = \nu_1$ type-1 Fermi resonance as well as a $\nu_2 + \nu_1 = \nu_2$ type-2 Fermi resonance. Likewise, the NeDH⁺ and NeD₂⁺ systems require an additional $2\nu_3 = \nu_2$ type-1 Fermi resonance as well as a further $\nu_2 + \nu_3 = \nu_3$ type-2 Fermi resonance.

In the course of this study, it was found that the quartic terms for the π bending mode are unreliable due to the flatness of the PES in this coordinate coupled with only having one, with at most two, significant figures in the quartic force constants. As such, these terms are dropped from the definition of the PES giving a QFF for only the totally-symmetric modes (the two stretches) and a cubic force field PES for the pair of degenerate bending modes. Even so, all of the CcCR spectroscopic constants of the ground vibrational state are produced in the same manner and, subsequently, the same accuracy as those produced in the previous studies (Huang et al. 2011; Fortenberry et al. 2011a,b, 2012; Huang et al. 2013a), since only cubic terms are necessary for the computation of B_0 and the other desired spectroscopic constants in the first place (Gaw et al. 1991). Additionally, the ν_1 and ν_2 frequencies, as well as their vibrationally-averaged rotational constants, are defined and computed in the same procedure as has been previously benchmarked for high accuracy. The ν_3 frequency may not be as reliable since its largest contributor to the Taylor series definition of the potential is cubic, but this is still an improvement over simple harmonic frequencies and will give some indication as to the rotational structure of this vibrational state.

The vibrational frequencies for this noble gas compound are very different from “standard” atoms. For instance, the

ν_1 H–H stretch is over half the value of what is known for the stretching motion of hydrogen atom at more than 4000 cm⁻¹ or less than 2.5 microns (Irikura 2007), but actually quite close to the roughly 2000 cm⁻¹ (5.0 microns) fundamental vibrational frequency of H₂⁺ (Herzberg & Jungen 1972; Roth et al. 2008). As a result of these closely coincidental values, it is interpreted that the presence of the H–H bond behaves much like it does in the hydrogen molecular cation, but the neon atom affects this motion to a small degree indicating that some bonding is present. The ν_2 Ne–H stretch fundamental is substantially lower than most other heavy atom to hydrogen stretches, which are typically in the 3300 to 3600 cm⁻¹ (2.8 – 3.0 micron) region, but the harmonic frequency is many times higher than van der Waals Ne–X stretching frequencies (Grandinetti 2011) indicating that the Ne–H bond itself is also weak but certainly functional. Finally, the bending motion is also lower than it would be in most purely “covalent” structures. Hence, the vibrations of NeH₂⁺ imply that this molecule is weakly associated but has some level of electron sharing in its stabilization making it more than merely a van der Waals complex.

The bond lengths for NeH₂⁺ further indicate that this molecule is more than a van der Waals complex. The Ne–H bond is longer than other hydrogen bonds of the same period, but much shorter than would be found in purely electrostatic interactions between noble gases and ligands (Grandinetti 2011). The equilibrium bond lengths remain the same upon isotopomerization since the potential has been formulated, again, within the Born-Oppenheimer approximation. Similarly, the dipole moment remains unchanged for our set of computations. The CCSD(T)/aug-cc-pV5Z dipole moment computed from the centre-of-mass at the origin is very high here at 5.61 D making this cation very rotationally bright regardless of the isotopologue examined. The R_α vibrationally-averaged bond lengths are affected by the differences in the various isotopic masses as shown in Tables 2 and 3 which, in turn, influence the B -type rotational constants. Inclusion of the ²²Ne over ²⁰Ne lowers B_0 by 554.0 MHz, which will produce noticeably different rotational spectra at high enough resolution, but the near doubling of the hydrogen masses upon deuteration will have a much greater effect on any observed rotational lines. Also from the tables, the vibrational modes are all affected by isotopic shifts that further affects the B_1 , B_2 , and B_3 constants giving new rotational structure for the vibrationally excited states.

3.2 ArH₂⁺ Structural and Spectroscopic Considerations

The force constants for ²Σ⁺ ArH₂⁺ are given in Table 4 including, again, all positive second derivatives. Argon has three stable isotopes: ³⁶Ar, ³⁸Ar, and ⁴⁰Ar. ³⁶ArH⁺ was detected in the Crab nebula (Barlow et al. 2013), even though ⁴⁰Ar is the more abundant isotope on Earth. The reasons for the difference in abundances of the two isotopes have been well documented (Cueto et al. 2014), but inclusion of all three forms of argon is warranted in this study for the sake of completeness. The structural, spectroscopic, and vibrational values for the twelve different isotopologues (including deuteration) are given in Tables 5, 6, and 7.

The resonances required for the SPECTRO computa-

tions are not affected by inclusion of the different argon isotopes. However, the deuteration affects these necessary inputs since it influences the rovibrational structure of the molecules more noticeably. No resonances of any kind are needed for ArH_2^+ . The resonances required for ArHD^+ include a $2\nu_2 = \nu_1$ type-1 Fermi resonance, a $\nu_2 + \nu_1 = \nu_2$ type-2 Fermi resonance, and ν_2/ν_3 Coriolis resonances. ArDH^+ is reliant upon $2\nu_3 = \nu_1$ and $2\nu_3 = \nu_2$ type-1 Fermi resonances, a $\nu_2 + \nu_3 = \nu_3$ type-2 Fermi resonance, and a ν_2/ν_1 Darling-Dennison resonance. The ArD_2^+ resonances are the same as those for ArDH^+ but without the Darling-Dennison resonance. A similar issue with the quartic terms of the π -bending coordinate were also encountered with ArH_2^+ leading once again to the use of the CcCR QFF for the totally-symmetric terms but only the CcCR cubic force field for the bending mode(s).

The Born-Oppenheimer dipole moment computed from the centre-of-mass for ArH_2^+ is not as high as it is for the neon compound but still quite significant at 4.37 D. The Ar–H bond length is around 1.44 Å for each isotopologue, which is about 0.1 Å longer than another set of third-row atom containing compounds, *cis*- and *trans*-HSCO, where the S–H bond lengths are 1.34–1.35 Å (Fortenberry et al. 2014). Even so, it is still in the range of fairly well bonded hydrogen atoms for larger atoms of this size and cannot be interpreted as a van der Waals complex, even though the equilibrium H–H bond length of 1.110 Å is very close to the 1.053 Å bond length in H_2^+ (Herzberg & Jungen 1972).

The anharmonic vibrational frequencies for the ArH_2^+ isotopologues are significantly less than their neon-containing counterparts, as one would expect for inclusion of a heavier atom—argon in this case. However, the decrease in the H–H stretch from 1801.5 cm^{-1} (5.551 microns) in the standard isotopologue of NeH_2^+ to 1229.8 cm^{-1} (8.131 microns) in $^{36}\text{ArH}_2^+$ indicates that this bond is even more perturbed by the presence of the argon than the neon when compared to mere H_2^+ . The ν_2 Ar–H stretch is 201.7 cm^{-1} less at 590.5 cm^{-1} (16.93 microns) than the $^{20}\text{NeH}_2^+$ ν_2 Ne–H stretch. However, this mode is strongly anharmonic for ArH_2^+ , where the anharmonicities are on the order of 500 cm^{-1} . Single deuteration of the terminal hydrogen significantly reduces the anharmonicities, on the order of a half, and the ArDH^+ ν_2 stretches are almost harmonic in comparison. Also, the ν_2 Ar–H stretch is significantly lower in ArH_2^+ than it is in ArH^+ where the frequency is 2592.65 cm^{-1} or 3.857 microns (Cueto et al. 2014) indicating that the Ar–H bond is stronger in the diatomic cation than it is in ArH_2^+ . However, the 590.5 cm^{-1} ν_2 Ar–H stretch is notably higher than the comparable 350 cm^{-1} Ar–H₂ stretch observed for the ArH_2 neutral van der Waals complex (McKellar 1996). The exception to the decrease in frequency for the ArH_2^+ fundamentals as compared to NeH_2^+ is the π -bending mode. For the standard isotopologue, the NeH_2^+ bending mode is 98.5 cm^{-1} less than its $^{36}\text{ArH}_2^+$ counterpart. However, again, the lack of quartic terms in these descriptions does not lend strong credence to any conclusions taken about these modes besides a general location as to where these bending frequencies can be found.

The vibrational frequencies indicate that ArH_2^+ is not quite as strongly bound as ArH^+ but is more strongly associated than neutral ArH_2 . This is corroborated by the force constants, which, according to Badger’s Law, indicate

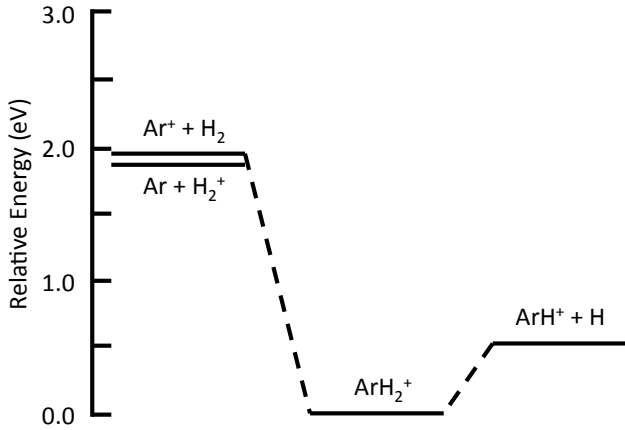
bond strength since it is proportional to the force constant of the vibration. From Table 4, the F_{11} force constant corresponds to the Ar–H stretch and is 1.895 279 mdyne/Å. Using the harmonic approximation from the vibrational frequency derived by Cueto et al. (2014) (2592.65 cm^{-1}), the ArH^+ force constant is 3.883 866 mdyne/Å, nearly double that in ArH_2^+ . Concurrently, the F_{22} force constant is 0.700 608 mdyne/Å indicating that the H–H bond is half as strong as it is in H_2^+ , where the harmonic force constant is 1.425 879 mdyne/Å from a 2191.13 cm^{-1} frequency (Roth et al. 2008). Regardless of the strength of the bonds and the degree to which electrons are shared between the Ar atom and the H_2^+ cation, the rotational constants and other spectroscopic data for ArH_2^+ as provided in Tables 5, 6, and 7 can be applied to spectral analysis of the ISM or simulated laboratory experiments.

3.3 Astrochemical Pathways and Spectra

The main question regarding the detectability of these compounds in the ISM or their presence in interstellar chemical pathways is whether or not these structures are stable and, if so, by how much. Since zero gradients are determined along with positive second derivatives (See Tables 1 and 4) these structures are minima on their respective potential surfaces. In fact, these $^2\Sigma^+$ linear structures are the global minima on their respective PESs. In Table 8, the major possible dissociation pathways are listed for each noble gas molecule with energies provided relative to each triatomic minimum. According to “gold standard” (Helgaker et al. 2004) CCSD(T)/aug-cc-pVTZ computations, the most likely direct dissociation pathway for NeH_2^+ is into the Ne atom and the hydrogen molecular cation. The NeH_2^+ minimum sits 0.560 eV below these two products. All the fundamental vibrational frequencies are below this value showing that vibrational transitions, in addition to pure rotational spectra, can be detected for this system if the conditions are correct for its interstellar formation. The next-lowest dissociation pathway is for NeH_2^+ to lose a hydrogen atom to form NeH^+ , but this costs nearly twice as much energy at 1.031 eV. This closely mirrors the previous $\text{Ne} + \text{H}_2^+ \rightarrow \text{NeH}^+ + \text{H}$ PES computed by Gamallo et al. (2013) and shown in Figure 1 therein.

The energetics of these two pathways are reversed for ArH_2^+ , which is the global minimum on its PES. The lowest energy dissociation pathway is, again from Table 8, into ArH^+ and a hydrogen atom where only 0.493 eV is required to break the triatomic noble gas cation down. The dissociation into the Ar atom and hydrogen molecular cation is much higher at 1.838 eV and further breakdown into $\text{Ar} + \text{H} + \text{H}^+$ requires another 2.429 eV, comparable to 2.634 eV predicted by Song & Gisalson (2003) with a lower level of theory. Since the most likely way for ArH_2^+ to dissociate, and do so by a wide margin, is to form ArH^+ and a hydrogen atom, it seems likely that ArH_2^+ is a precursor to the formation of ArH^+ in the $\text{ArH}^+ + \text{H}_2$ PES. Since this dissociation energy corresponds to an equivalent temperature of 5725.7 K, hot regions like the Crab nebula where ArH^+ has been detected should see ArH_2^+ break down fairly easily into the previously detected ArH^+ diatomic cation. Cooler regions, such as molecular clouds, should retain a fair amount of ArH_2^+ before dissociation into ArH^+ .

Figure 1. Visual depiction for the relative energies of the ArH₂⁺ PES.

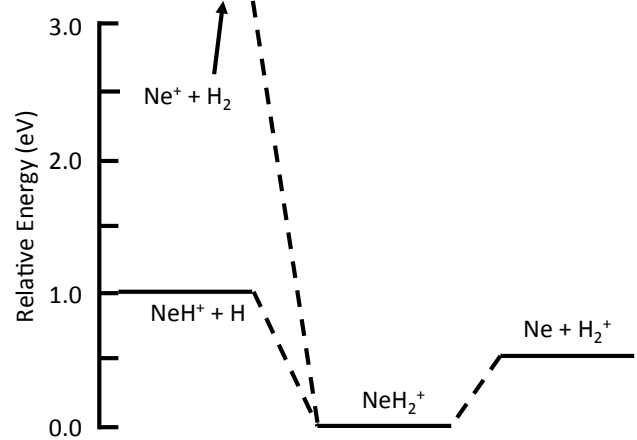


Therefore, it is plausible that ArH⁺ forms, at least in part, from ArH₂⁺ in the ISM. It may be that ArH₂⁺ is the necessary stable or semi-stable intermediate in the Ar⁺ + H₂ → ArH⁺ + H mechanism as proposed by Barlow et al. (2013) since formation of ArH₂⁺ from Ar⁺ + H₂ produces 1.930 eV (see Table 8) of energy whereas direct, bimolecular dissociation produces 1.436 eV. Granted, 0.493 eV must be imparted into the system to break ArH₂⁺ down into ArH⁺ + H, but this stabilization brought about by the presence of ArH₂⁺ in the reaction scheme may speed up the formation of ArH⁺ in the ISM. Additionally, the role of ArH₂⁺ may also be an intermediate in the alternative Ar + H₂⁺ → ArH⁺ + H mechanism, as well, which is slightly more energetically favorable at 1.838 eV above the ArH₂⁺ minimum. These possible reactions schemes are depicted in Figure 1. Additionally, ArH₂⁺ may even be a simple degradation precursor to ArH⁺ in cool environments after collision with another body. Regardless, ArH₂⁺ should be detectable, even if in small amounts as it would be functioning as an intermediate, due to its large dipole moment. Finally, NeH⁺ will probably not be as abundant as ArH⁺ as has been shown recently (Schilke et al. 2014). The most probable dissociation pathway for NeH₂⁺ is into Ne and H₂⁺, as depicted in Figure 2 corroborating previous work on this PES (Gamallo et al. 2013), making any potential NeH⁺ detection unlikely. This is especially true if the Ne⁺ + H₂ reaction is necessary to create NeH⁺ as it has been suggested for Ar⁺ + H₂ to form ArH⁺ (Barlow et al. 2013; Schilke et al. 2014; Roueff et al. 2014).

If detected as a stable species in its own right, ArH₂⁺ could also serve as a contributing factor indicating the temperature of a given warm astronomical environment since it should dissociate around 5700 K. Even though its most likely dissociation energy is at an equivalent temperature of 6500 K, NeH₂⁺ is not as flexible for use as a thermometer. Again, its primary dissociation pathway is into the neutral noble gas atom and H₂⁺. No rotationally bright product is created that could be interpreted as unique to NeH₂⁺ dissociation as it is in ArH₂⁺ → ArH⁺ + H.

The rotational spectra of NeH₂⁺ and ArH₂⁺ can be produced from the spectroscopic data provided herein. Due to its potential relationship of ArH₂⁺ to ArH⁺, the rota-

Figure 2. Visual depiction for the relative energies of the NeH₂⁺ PES.



tional spectrum of NeH₂⁺ is left to the reader to deduce. The natural [³⁶Ar/³⁸Ar] ratio of roughly 5.25 should produce a sizable intensity for the rotational transitions of the heavier isotopologue of ArH₂⁺ in addition to the stronger ³⁶ArH₂⁺ rotational lines. Figure 3 demonstrates what the full rotational spectrum for ArH₂⁺ should look like at 40 K with the intensities of ³⁶ArH₂⁺ normalized and the intensities of ³⁸ArH₂⁺ scaled from the permanent dipole moment and the relative natural abundance of ³⁸Ar. The simple model linear rotor for inclusion of up to sextic distortion,

$$\Delta E(J+1 \rightarrow J) = 2B(J+1) - 4D(J+1)^3 + H(J+1)^3 [(J+2)^3 - J^3], \quad (2)$$

is employed here within the PGOPHER (Western 2013) program making use of the spectroscopic constants given in Tables 5 and 6. Transitions up to the $J = 10 \rightarrow 9$ line located just around 1.2 THz should be visible, but the $J = 4 \rightarrow 3$ line appears to be the brightest at these temperatures.

At temperatures closer to that found in the Crab nebula or similar environments, the spectrum changes markedly, as depicted in Figure 4 for 5000 K. In addition to the increase in the number of pure rotational lines present, the vibrationally excited states are substantially more populated at this temperature with Boltzmann proportions of 0.71, 0.84, and 0.83, respective of ν_1 , ν_2 , and ν_3 , normalized to the pure rotational transitions. As such, the spectrum becomes more complicated in this idealized depiction. The $J = 42 \rightarrow 41$ transition is the brightest at this temperature and should be found in the 4.9 THz range. The spin-orbit peak splitting present in such radicals is not modeled here due to limitations in our methodology but would be a further factor in the interstellar detection of these noble gas-containing triatomic cations regardless of the environmental temperatures.

To aid in experimental characterization, the pure rotational line list for $\Delta E(J+1 \rightarrow J)$, $J \leq 9$, of the most abundant isotopes of argon, ³⁶Ar and ³⁸Ar, is given in Table 9 to complement Figures 3 and 4. Experience has shown that the rotational constants may vary from experiment by 10-25 MHz. As such the variance from experiment for the lines listed here will grow for higher J , but the relative transition frequencies and the relative intensities will, no doubt, benefit searches for this noble gas cation.

Figure 3. The rotational spectrum of the ground and excited vibrational states of ArH_2^+ in THz at 40 K with the shorter lines corresponding to $^{38}\text{ArH}_2^+$ and the taller lines to $^{36}\text{ArH}_2^+$ based on the relative natural abundances of the argon isotopes.

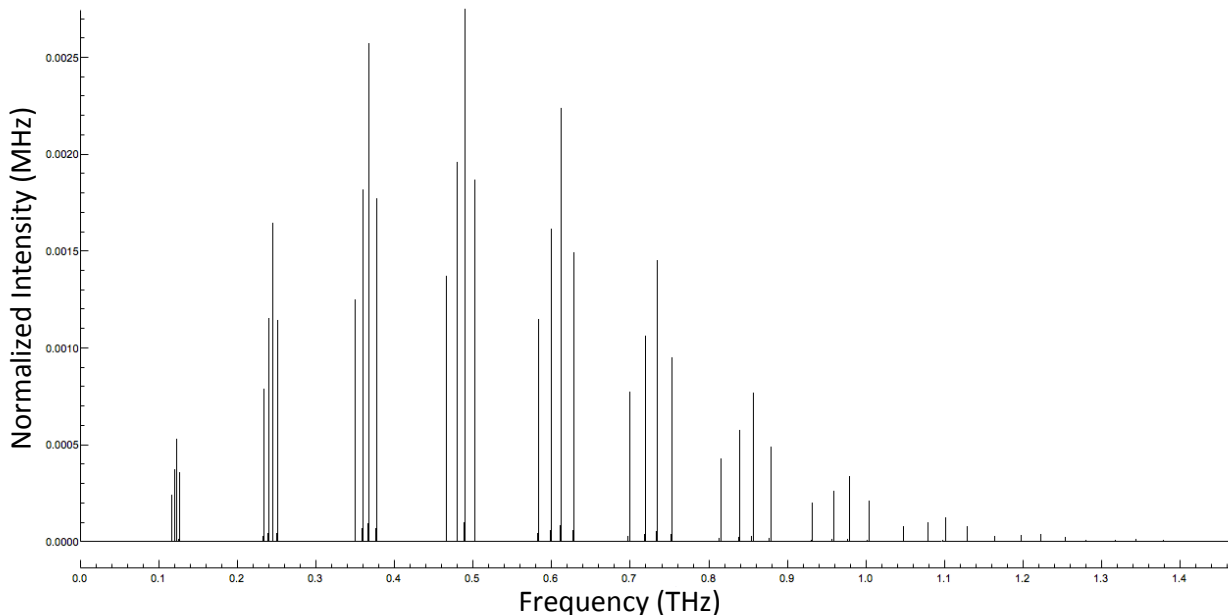
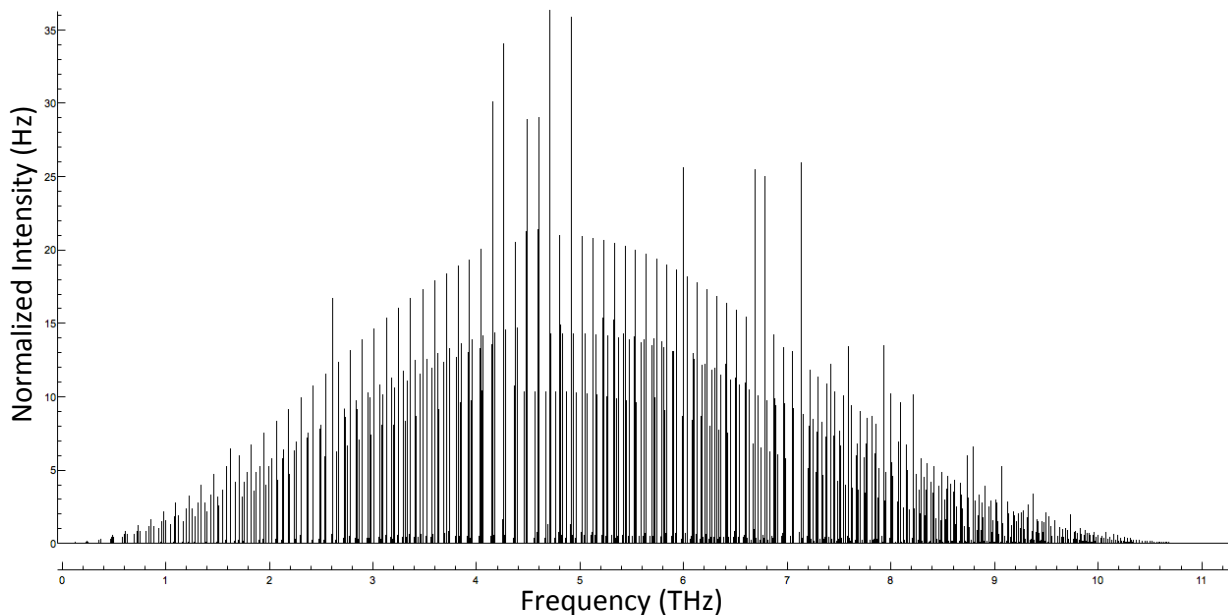


Figure 4. The rotational spectrum of ArH_2^+ in THz at 5000 K where the vibrationally excited rotational lines of $^{36}\text{ArH}_2^+$ and $^{38}\text{ArH}_2^+$ are visible.



4 CONCLUSIONS

The rotational and rovibrational spectroscopic data provided here should assist in the potential detection of NeH_2^+ and ArH_2^+ in the ISM. The pure rotational and ν_1/ν_2 data are computed in the same CcCR QFF fashion as has been done previously to produce highly-accurate results. Since the π -bending mode could not fully employ this same approach, the spectroscopic data generated by the cubic force field will certainly provide deeper insight into the vibrational and

rovibrational nature of the ν_3 modes than harmonically derived values can. The bond lengths and vibrational frequencies show clear demarcation from simple van der Waals complexes for these two noble gas cations. NeH_2^+ and ArH_2^+ are more covalent in nature but cannot be considered purely covalent. Both species exhibit large dipole moments that should make them more easily detected than other “trace” species in the ISM.

Additionally, the different lowest-energy CCSD(T)/aug-cc-pVTZ dissociation pathways of NeH_2^+

into Ne and H₂⁺ with ArH₂⁺ into ArH⁺ and H showcase the differences in the two noble gas atoms. It is therefore likely that ArH₂⁺ is a precursor to ArH⁺ as a reaction intermediate between Ar + H₂⁺ or Ar⁺ + H₂ where ArH⁺ and a hydrogen atom are the major products. In either case, ArH₂⁺ is the global minimum on the PES. If ArH₂⁺ is involved in the formation of ArH⁺, it is unlikely, then, that NeH⁺ will form in the ISM in a similar fashion since this is not the most energetically favorable pathway. As a result, detection of the neon hydride cation is doubtful as recent surveys have shown (Schilke et al. 2014). Regardless, the reference data provided here, including the rotational spectra, should assist in analysis of the noble gas chemistry of the Crab nebula where ArH⁺ has been detected or in other regions in which other noble gas compounds may be observed.

5 ACKNOWLEDGEMENTS

The authors are grateful to Georgia Southern University for providing start-up funds that supported this research in the form of student salaries and the purchase of computer equipment. The Georgia Southern College of Science and Mathematics also provided support for WJM and RCF from an “Interdisciplinary Pilot Grant”. This work used the Extreme Science and Engineering Discovery Environment (XSEDE), which is supported by National Science Foundation grant number ACI-1053575. The authors would also like to thank Jim LoBue of Georgia Southern for providing many of the references cited as well as Mallory L. Theis and Lauren F. Fortenberry for assistance in editing the manuscript. Prof. Jonathan Tennyson of the University College London is gratefully thanked for pointing out a systemic error in our original spectra that has since been corrected. The reviewer is also acknowledged for the very useful insights provided throughout the review process.

REFERENCES

- Adams N. G., Bohme D. K., Ferguson E. E., 1970, *J. Chem. Phys.*, 52, 5101
- Allen W. D., coworkers, *INTDER 2005 is a General Program, which Performs Vibrational Analysis and Higher-Order Non-Linear Transformations*, 2005
- Barletta P., 2009, *Eur. Phys. J. D*, 53, 33
- Barlow M. J., Swinyard B. M., Owen P. J., Cernicharo J., Gomez H. L., Ivison R. J., Krause O., Lim T. L., Matsumura M., Miller S., Olofsson G., Polehampton E. T., 2013, *Science*, 342, 1343
- Bartl P., Leidlmair C., Denifl S., Scheier P., Echt O., 2013, *Chem. Phys. Chem.*, 14, 227
- Bedford D. K., Smith D., 1990, *Int. J. Mass Spectrom. Ion Proc.*, 98, 179
- Borocci S., Giordani M., Grandinetti F., 2011, *Comput. Theor. Chem.*, 964, 318
- Cueto M., Cernicharo J., Barlow M. J., Swinyard B. M., Herrero V. J., Tanarro I., Doménech J. L., 2014, *Astrophys. J.*, 78, L5
- Douglas M., Kroll N., 1974, *Ann. Phys.*, 82, 89
- Dunning T. H., 1989, *J. Chem. Phys.*, 90, 1007
- Fortenberry R. C., Huang X., Francisco J. S., Crawford T. D., Lee T. J., 2011a, *J. Chem. Phys.*, 135, 134301
- Fortenberry R. C., Huang X., Francisco J. S., Crawford T. D., Lee T. J., 2011b, *J. Chem. Phys.*, 135, 214303
- Fortenberry R. C., Huang X., Francisco J. S., Crawford T. D., Lee T. J., 2012, *J. Chem. Phys.*, 136, 234309
- Fortenberry R. C., Huang X., McCarthy M. C., Crawford T. D., Lee T. J., 2014, *J. Phys. Chem. B*, 118, 6498
- Fortenberry R. C., Huang X., Yachmenev A., Thiel W., Lee T. J., 2013, *Chem. Phys. Lett.*, 574, 1
- Gamallo P., Huarte-Larrañaga F., González M., 2013, *J. Phys. Chem. A*, 117, 5393
- Gauss J., Lauderdale W. J., Stanton J. F., Watts J. D., Bartlett R. J., 1991, *Chem. Phys. Lett.*, 182, 207
- Gaw J. F., Willets A., Green W. H., Handy N. C., 1991, in Bowman J. M., Ratner M. A., eds, *Advances in Molecular Vibrations and Collision Dynamics*. JAI Press, Inc., Greenwich, Connecticut, pp 170–185
- Grandinetti F., 2011, *Eur. J. Mass Spectrom.*, 17, 423
- Helgaker T., Ruden T. A., Jørgensen P., Olsen J., Klopper W., 2004, *J. Phys. Org. Chem.*, 17, 913
- Herzberg G., Jungen C., 1972, *J. Molec. Spectrosc.*, 41, 425
- Huang X., Fortenberry R. C., Lee T. J., 2013a, *J. Chem. Phys.*, 139, 084313
- Huang X., Fortenberry R. C., Lee T. J., 2013b, *Astrophys. J. Lett.*, 768, 25
- Huang X., Lee T. J., 2008, *J. Chem. Phys.*, 129, 044312
- Huang X., Lee T. J., 2009, *J. Chem. Phys.*, 131, 104301
- Huang X., Taylor P. R., Lee T. J., 2011, *J. Phys. Chem. A*, 115, 5005
- Irikura K. K., 2007, *J. Phys. Chem. Ref. Data*, 36, 389
- Kendall R. A., Dunning T. H., Harrison R. J., 1992, *J. Chem. Phys.*, 96, 6796
- Kim S. T., Lee J. S., 1999, *J. Chem. Phys.*, 110, 4413
- Lauderdale W. J., Stanton J. F., Gauss J., Watts J. D., Bartlett R. J., 1991, *Chem. Phys. Lett.*, 187, 21
- McCarthy M. C., Travers M. J., Kovács A., Gottlieb C. A., Thaddeus P., 1997, *Astrophys. J. Suppl. Ser.*, 113, 105
- McKellar A. R. W., 1996, *J. Chem. Phys.*, 105, 2628
- McKellar A. R. W., 2005, *J. Chem. Phys.*, 122, 084320
- McKellar A. R. W., 2009, *Can. J. Phys.*, 87, 411
- Martin J. M. L., Lee T. J., 1996, *Chem. Phys. Lett.*, 258, 136
- Martin J. M. L., Taylor P. R., 1994, *Chem. Phys. Lett.*, 225, 473
- Mayneris J., Sierra J. D., González M., 2008, *J. Chem. Phys.*, 128, 194307
- Mills I. M., 1972, in Rao K. N., Mathews C. W., eds, *Molecular Spectroscopy - Modern Research*. Academic Press, New York, pp 115–140
- Müller H. S., Schlöder F., Stutzki J., Winniewisser G., 2005, *J. Molec. Struct.*, 742, 215
- Papoušek D., Aliev M. R., 1982, *Molecular Vibration-Rotation Spectra*. Elsevier, Amsterdam
- Pauzat F., Ellinger Y., Pilmè J., Mousis O., 2009, *J. Chem. Phys.*, 130, 174313
- Pavanello M., Adamowicz L., Alijah A., Zobov N. F., Mizus I. I., Polyansky O. L., Tennyson J., Szidarovszky T., Császár A. G., Berg M., Petrigiani A., Wolf A., 2012, *Phys. Rev. Lett.*, 108, 023002
- Peterson K. A., Dunning T. H., 1995, *J. Chem. Phys.*, 102, 2032

Table 1. The NeH_2^+ CcCR Simple-Internal Force Constants (in $\text{mdyn}/\text{\AA}^n \cdot \text{rad}^m$)^a.

F ₁₁	1.039 234	F ₃₃₁	-0.1783	F ₃₃₁₁	0.13
F ₂₁	0.383 519	F ₃₃₂	-0.0352	F ₃₃₂₁	0.39
F ₂₂	1.197 493	F ₄₄₁	-0.1783	F ₃₃₂₂	0.37
F ₃₃	0.061 686	F ₄₄₂	-0.0352	F ₃₃₃₃	-1.72
F ₄₄	0.061 686	F ₁₁₁₁	52.85	F ₄₄₁₁	0.13
F ₁₁₁	-7.9408	F ₂₁₁₁	5.13	F ₄₄₂₁	0.39
F ₂₁₁	-1.7665	F ₂₂₁₁	2.45	F ₄₄₂₂	0.37
F ₂₂₁	-0.0664	F ₂₂₂₁	-0.59	F ₄₄₃₃	-0.49
F ₂₂₂	-5.7851	F ₂₂₂₂	25.68	F ₄₄₄₄	-1.72

^a1 $\text{mdyn} = 10^{-8}$ N; n and m are exponents corresponding to the number of units from the type of modes present in the specific force constant. \AA are fitting for modes of bond stretches and degrees for the degenerate bending modes.

- Raghavachari K., Trucks. G. W., Pople J. A., Head-Gordon M., 1989, Chem. Phys. Lett., 157, 479
- Roth B., Koelemeij J., Schiller S., Hilico L., Karr J.-P., Korobov V., Bakalov D., 2008, in Karshenboim S. G., ed., Lecture Notes in Physics 745: Precision Physics of Simple Atoms and Molecules. Springer, New York
- Roueff E., Alekseyev A. B., Bourlot J. L., 2014, Astron. Astrophys., 566, A30
- Schilke P., Neufeld D. A., Müller H. S. P., et al., 2014, Astron. Astrophys., 566, A29
- Song J.-B., Gisalson E. A., 2003, Chem. Phys., 293, 231
- Tosi P., Dmitrijev O., Soldo Y., Bassi D., Cappelletti D., Pirani F., Aquilanti V., 1993, J. Chem. Phys., 99, 985
- Turney J. M., Simmonett A. C., Parrish R. M., et al., 2012, Wiley Interdisc. Rev. Comput. Molec. Sci., 2, 556
- Watson J. K. G., 1977, in During J. R., ed., Vibrational Spectra and Structure. Elsevier, Amsterdam, pp 1–89
- Watts J. D., Gauss J., Bartlett R. J., 1993, J. Chem. Phys., 98, 8718
- Werner H.-J., Knowles P. J., Knizia G., Manby F. R., Schütz M., et al., 2012, MOLPRO, version 2012.1, a package of *ab initio* programs
- Western C. M., PGOHPER, a Program for Simulating Rotational Structure, University of Bristol, <http://pgopher.chm.bris.ac.uk>, 2013

Table 2. The CcCR Zero-Point (R_α vibrationally-averaged) and Equilibrium Structures, Rotational Constants, CCSD(T)/aug-cc-pV5Z Dipole Moment, Vibration-Rotation Interaction Constants, and Quartic (D, τ) and Sextic (H) Distortion Constants of ²⁰NeH₂⁺ and Deuterated Isotopologues.

	NeH ₂ ⁺	NeHD ⁺	NeDH ⁺	NeD ₂ ⁺
$r_0(\text{Ne-H}_1)$	1.234 314 Å	1.231 167 Å	1.230 908 Å	1.228 534 Å
$r_0(\text{H}_1\text{-H}_2)$	1.105 287 Å	1.105 987 Å	1.101 895 Å	1.104 149 Å
B_0	78 699.8 MHz	46 203.8 MHz	67 591.3 MHz	42 820.6 MHz
α^B 1	2406.6 MHz	2444.3 MHz	36.8 MHz	949.2 MHz
α^B 2	3745.6 MHz	1329.0 MHz	3324.5 MHz	1474.6 MHz
α^B 3	-1494.2 MHz	-1066.2 MHz	-573.0 MHz	-572.8 MHz
τ_{aaaa}	-9.417 MHz	-3.037 MHz	-7.795 MHz	-2.735 MHz
$r_e(\text{Ne-H}_1)$	1.211 598 Å	–	–	–
$r_e(\text{H}_1\text{-H}_2)$	1.100 735 Å	–	–	–
B_e	80 281.7 MHz	47 024.2 MHz	68 698.9 MHz	43 459.7 MHz
D_e	2.354 MHz	0.759 MHz	1.949 MHz	0.684 MHz
H_e	-49.825 Hz	-3.043 Hz	-63.774 Hz	-7.235 Hz
μ_z^a	5.61 D	–	–	–
$\omega_1(\sigma)$ H–H	1907.4 cm ⁻¹	1722.9 cm ⁻¹	1634.8 cm ⁻¹	1349.8 cm ⁻¹
$\omega_2(\sigma)$ Ne–H	970.4 cm ⁻¹	777.1 cm ⁻¹	819.0 cm ⁻¹	716.9 cm ⁻¹
$\omega_3(\pi)$ Bend	633.7 cm ⁻¹	599.0 cm ⁻¹	495.6 cm ⁻¹	450.3 cm ⁻¹
Harmonic Zero-Point	2072.6 cm ⁻¹	1849.0 cm ⁻¹	1722.5 cm ⁻¹	1483.7 cm ⁻¹
$\nu_1(\sigma)$ H–H	1801.5 cm ⁻¹	1611.3 cm ⁻¹	1526.2 cm ⁻¹	1323.3 cm ⁻¹
$\nu_2(\sigma)$ Ne–H	792.2 cm ⁻¹	636.6 cm ⁻¹	723.2 cm ⁻¹	616.0 cm ⁻¹
$\nu_3(\pi)$ Bend	557.1 cm ⁻¹	530.3 cm ⁻¹	448.6 cm ⁻¹	404.8 cm ⁻¹
Zero-Point	2002.0 cm ⁻¹	1794.0 cm ⁻¹	1672.8 cm ⁻¹	1448.5 cm ⁻¹
B_1	76 293.2 MHz	43 759.50 MHz	67 554.50 MHz	41 871.40 MHz
B_2	74 954.2 MHz	44 874.80 MHz	64 266.80 MHz	41 346.00 MHz
B_3	80 194.0 MHz	46 778.40 MHz	68 164.30 MHz	43 393.30 MHz

^aThe NeH₂⁺ coordinates (in Å with the centre-of-mass at the origin) used to generate the Born-Oppenheimer dipole moment component are: Ne, 0.000000, 0.000000, -0.161373; H₁, 0.000000, 0.000000, 1.050226; H₂, 0.000000, 0.000000, 2.150962

Table 3. The CcCR ²²NeH₂⁺ and Deuterated Isotopologues Spectroscopic Data.

	NeH ₂ ⁺	NeHD ⁺	NeDH ⁺	NeD ₂ ⁺
$r_0(\text{Ne-H}_1)$	1.234 199 Å	1.231 038 Å	1.230 760 Å	1.228 380 Å
$r_0(\text{H}_1\text{-H}_2)$	1.105 262 Å	1.105 968 Å	1.101 848 Å	1.104 113 Å
B_0	78 115.8 MHz	45 698.4 MHz	66 882.8 MHz	42 241.2 MHz
α^B 1	2382.0 MHz	2412.4 MHz	30.2 MHz	931.2 MHz
α^B 2	3707.2 MHz	1309.7 MHz	3274.4 MHz	1447.6 MHz
α^B 3	-1482.8 MHz	-1054.4 MHz	-566.4 MHz	-564.8 MHz
τ_{aaaa}	-9.283 MHz	-2.972 MHz	-7.646 MHz	-2.665 MHz
$r_e(\text{Ne-H}_1)$	1.211 598 Å	–	–	–
$r_e(\text{H}_1\text{-H}_2)$	1.100 735 Å	–	–	–
B_e	79 677.6 MHz	46 505.0 MHz	67 968.6 MHz	42 865.8 MHz
D_e	2.321 MHz	0.743 MHz	1.912 MHz	0.666 MHz
H_e	-49.088 Hz	-3.014 Hz	-62.171 Hz	-7.058 Hz
$\omega_1(\sigma)$ H–H	1907.4 cm ⁻¹	1722.6 cm ⁻¹	1634.8 cm ⁻¹	1349.7 cm ⁻¹
$\omega_2(\sigma)$ Ne–H	966.4 cm ⁻¹	777.6 cm ⁻¹	814.1 cm ⁻¹	711.4 cm ⁻¹
$\omega_3(\pi)$ Bend	633.5 cm ⁻¹	598.7 cm ⁻¹	495.2 cm ⁻¹	449.9 cm ⁻¹
Harmonic Zero-Point	2070.4 cm ⁻¹	1848.8 cm ⁻¹	1719.7 cm ⁻¹	1480.5 cm ⁻¹
$\nu_1(\sigma)$ H–H	1800.6 cm ⁻¹	1610.6 cm ⁻¹	1525.7 cm ⁻¹	1320.2 cm ⁻¹
$\nu_2(\sigma)$ Ne–H	790.0 cm ⁻¹	633.7 cm ⁻¹	719.6 cm ⁻¹	612.4 cm ⁻¹
$\nu_3(\pi)$ Bend	557.0 cm ⁻¹	530.3 cm ⁻¹	448.5 cm ⁻¹	404.6 cm ⁻¹
Zero-Point	1999.8 cm ⁻¹	1791.5 cm ⁻¹	1670.1 cm ⁻¹	1445.5 cm ⁻¹
B_1	75 733.8 MHz	43 286.0 MHz	66 852.6 MHz	41 310.0 MHz
B_2	74 408.5 MHz	44 388.6 MHz	63 608.4 MHz	40 793.6 MHz
B_3	74 408.5 MHz	46 752.8 MHz	67 449.2 MHz	42 806.1 MHz

Table 4. The ArH_2^+ CcCR Simple-Internal Force Constants (in $\text{mdyn}/\text{\AA}^n\text{-rad}^m$)^a.

F ₁₁	1.895 279	F ₃₃₁	-0.1878	F ₃₃₁₁	-8.29
F ₂₁	0.621 557	F ₃₃₂	0.0940	F ₃₃₂₁	1.67
F ₂₂	0.700 608	F ₄₄₁	-0.1878	F ₃₃₂₂	-46.58
F ₃₃	0.077 729	F ₄₄₂	0.0940	F ₃₃₃₃	-101.03
F ₄₄	0.077 729	F ₁₁₁₁	56.65	F ₄₄₁₁	-8.29
F ₁₁₁	-11.0653	F ₂₁₁₁	1.31	F ₄₄₂₁	1.67
F ₂₁₁	-1.5955	F ₂₂₁₁	-3.62	F ₄₄₂₂	-46.58
F ₂₂₁	-0.5609	F ₂₂₂₁	0.64	F ₄₄₃₃	-33.57
F ₂₂₂	-3.6640	F ₂₂₂₂	9.06	F ₄₄₄₄	-101.03

^a1 $\text{mdyn} = 10^{-8}$ N; see Figure 1 footnote *a* for more details.**Table 5.** The CcCR Zero-Point (R_α vibrationally-averaged) and Equilibrium Structures, Rotational Constants, CCSD(T)/aug-cc-pV5Z Dipole Moment, Vibration-Rotation Interaction Constants, and Quartic (D, τ) and Sextic (H) Distortion Constants of $^{36}\text{ArH}_2^+$ and Deuterated Isotopologues.

	ArH_2^+	ArHD^+	ArDH^+	ArD_2^+
$r_0(\text{Ar}-\text{H}_1)$	1.441 869 \AA	1.442 966 \AA	1.438 876 \AA	1.440121 \AA
$r_0(\text{H}_1-\text{H}_2)$	1.120 932 \AA	1.113 211 \AA	1.123 344 \AA	1.117636 \AA
B_0	61 278.8 MHz	35 878.2 MHz	50 663.7 MHz	32 232.2 MHz
α^B 1	2924.3 MHz	1801.9 MHz	1093.0 MHz	1060.7 MHz
α^B 2	1246.7 MHz	839.5 MHz	900.6 MHz	497.6 MHz
α^B 3	-1575.0 MHz	-1132.0 MHz	-670.9 MHz	-585.2 MHz
τ_{aaaa}	-3.199 MHz	-1.235 MHz	-2.015 MHz	-0.886 MHz
$r_e(\text{Ar}-\text{H}_1)$	1.434 944 \AA	–	–	–
$r_e(\text{H}_1-\text{H}_2)$	1.110 007 \AA	–	–	–
B_e	61 789.3 MHz	36 066.8 MHz	50 989.6 MHz	32 426.2 MHz
D_e	0.800 MHz	0.309 MHz	0.511 MHz	0.221 MHz
H_e	4.999 Hz	-0.267 Hz	2.132 Hz	0.690 Hz
μ_z^a	4.37 D	–	–	–
$\omega_1(\sigma)$ H–H	1531.3 cm^{-1}	1529.3 cm^{-1}	1121.1 cm^{-1}	1095.7 cm^{-1}
$\omega_2(\sigma)$ Ar–H	1096.6 cm^{-1}	787.0 cm^{-1}	1073.4 cm^{-1}	787.0 cm^{-1}
$\omega_3(\pi)$ Bend	665.0 cm^{-1}	623.8 cm^{-1}	524.6 cm^{-1}	471.3 cm^{-1}
Harmonic Zero-Point	1979.0 cm^{-1}	1782.0 cm^{-1}	1621.9 cm^{-1}	1412.7 cm^{-1}
$\nu_1(\sigma)$ H–H	1229.8 cm^{-1}	1333.7 cm^{-1}	1137.6 cm^{-1}	948.5 cm^{-1}
$\nu_2(\sigma)$ Ar–H	590.5 cm^{-1}	534.3 cm^{-1}	1044.1 cm^{-1}	591.6 cm^{-1}
$\nu_3(\pi)$ Bend	655.6 cm^{-1}	613.7 cm^{-1}	508.5 cm^{-1}	435.8 cm^{-1}
Zero-Point	1905.4 cm^{-1}	1735.6 cm^{-1}	1566.3 cm^{-1}	1381.3 cm^{-1}
B_1	58 354.6 MHz	34 076.2 MHz	49 570.7 MHz	31 171.4 MHz
B_2	60 032.1 MHz	35 038.7 MHz	49 763.1 MHz	31 734.6 MHz
B_3	62 853.9 MHz	37 010.2 MHz	51 334.6 MHz	31 756.7 MHz

^aThe ArH_2^+ coordinates (in \AA with the centre-of-mass at the origin) used to generate the Born-Oppenheimer dipole moment component are: Ar, 0.000000, 0.000000, -0.095551; H₁, 0.000000, 0.000000, 1.339394; H₂, 0.000000, 0.000000, 2.449401

Table 6. The $^{38}ArH_2^+$ and Deuterated Isotopologues CcCR Spectroscopic Data.

	ArH_2^+	$ArHD^+$	$ArDH^+$	ArD_2^+
$r_0(Ar-H_1)$	1.441 848 Å	1.442 947 Å	1.438 845 Å	1.440 092 Å
$r_0(H_1-H_2)$	1.120 940 Å	1.113 214 Å	1.123 355 Å	1.117 646 Å
B_0	61 121.6 MHz	35 740.9 MHz	50 475.8 MHz	32 075.6 MHz
α^B 1	2920.1 MHz	1797.3 MHz	1082.3 MHz	1058.3 MHz
α^B 2	1238.6 MHz	832.8 MHz	901.1 MHz	491.5 MHz
α^B 3	-1567.2 MHz	-1127.3 MHz	-668.3 MHz	-582.3 MHz
τ_{aaaa}	-3.182 MHz	-1.225 MHz	-2.029 MHz	-0.877 MHz
$r_e(Ar-H_1)$	1.434 944 Å	–	–	–
$r_e(H_1-H_2)$	1.110 007 Å	–	–	–
B_e	61 630.1 MHz	35 928.6 MHz	50 799.2 MHz	32 268.2 MHz
D_e	0.795 MHz	0.306 MHz	0.507 MHz	0.219 MHz
H_e	4.972 Hz	-0.257 Hz	2.094 Hz	0.684 Hz
$\omega_1(\sigma)$ H–H	1530.4 cm^{-1}	1528.3 cm^{-1}	1121.1 cm^{-1}	1094.3 cm^{-1}
$\omega_2(\sigma)$ Ar–H	1095.7 cm^{-1}	785.9 cm^{-1}	1071.3 cm^{-1}	785.8 cm^{-1}
$\omega_3(\pi)$ Bend	664.9 cm^{-1}	623.7 cm^{-1}	524.6 cm^{-1}	471.2 cm^{-1}
Harmonic Zero-Point	1978.0 cm^{-1}	1780.8 cm^{-1}	1620.8 cm^{-1}	1411.3 cm^{-1}
$\nu_1(\sigma)$ H–H	1228.6 cm^{-1}	1332.4 cm^{-1}	1139.2 cm^{-1}	946.8 cm^{-1}
$\nu_2(\sigma)$ Ar–H	591.6 cm^{-1}	534.0 cm^{-1}	1042.0 cm^{-1}	591.3 cm^{-1}
$\nu_3(\pi)$ Bend	655.6 cm^{-1}	613.7 cm^{-1}	508.7 cm^{-1}	435.8 cm^{-1}
Zero-Point	1904.5 cm^{-1}	1734.5 cm^{-1}	1565.1 cm^{-1}	1380.0 cm^{-1}
B_1	58 201.5 MHz	33 943.6 MHz	49 393.5 MHz	31 017.3 MHz
B_2	59 883.0 MHz	34 908.1 MHz	49 574.7 MHz	31 584.1 MHz
B_3	62 692.5 MHz	36 868.3 MHz	51 144.1 MHz	32 657.9 MHz

Table 7. The CcCR Spectroscopic Data for $^{40}ArH_2^+$ and Its Deuterated Isotopologues.

	ArH_2^+	$ArHD^+$	$ArDH^+$	ArD_2^+
$r_0(Ar-H_1)$	1.441 829 Å	1.442 930 Å	1.438 816 Å	1.440 066 Å
$r_0(H_1-H_2)$	1.120 946 Å	1.113 216 Å	1.123 364 Å	1.117 656 Å
B_0	60 979.5 MHz	35 616.8 MHz	50 306.0 MHz	31 934.2 MHz
α^B 1	2916.4 MHz	1793.1 MHz	1073.1 MHz	1056.0 MHz
α^B 2	1231.4 MHz	826.8 MHz	901.3 MHz	486.1 MHz
α^B 3	-1567.2 MHz	-1123.1 MHz	-666.0 MHz	-579.7 MHz
τ_{aaaa}	-3.166 MHz	-1.216 MHz	-2.015 MHz	-0.869 MHz
$r_e(Ar-H_1)$	1.434 944 Å	–	–	–
$r_e(H_1-H_2)$	1.110 007 Å	–	–	–
B_e	61 486.2 MHz	35 803.6 MHz	50 627.2 MHz	32 125.5 MHz
D_e	0.792 MHz	0.304 MHz	0.504 MHz	0.217 MHz
H_e	4.947 Hz	-0.248 Hz	2.061 Hz	0.678 Hz
$\omega_1(\sigma)$ H–H	1529.6 cm^{-1}	1527.4 cm^{-1}	1121.1 cm^{-1}	1093.1 cm^{-1}
$\omega_2(\sigma)$ Ar–H	1094.9 cm^{-1}	784.9 cm^{-1}	1069.3 cm^{-1}	784.8 cm^{-1}
$\omega_3(\pi)$ Bend	664.9 cm^{-1}	623.7 cm^{-1}	524.5 cm^{-1}	471.2 cm^{-1}
Harmonic Zero-Point	1977.2 cm^{-1}	1779.9 cm^{-1}	1619.7 cm^{-1}	1410.2 cm^{-1}
$\nu_1(\sigma)$ H–H	1214.8 cm^{-1}	1331.2 cm^{-1}	1140.5 cm^{-1}	945.2 cm^{-1}
$\nu_2(\sigma)$ Ar–H	592.5 cm^{-1}	533.7 cm^{-1}	1040.2 cm^{-1}	591.1 cm^{-1}
$\nu_3(\pi)$ Bend	655.6 cm^{-1}	613.6 cm^{-1}	508.8 cm^{-1}	435.8 cm^{-1}
Zero-Point	1904.0 cm^{-1}	1733.6 cm^{-1}	1564.0 cm^{-1}	1378.8 cm^{-1}
B_1	58 063.1 MHz	33 823.7 MHz	49 232.9 MHz	30 878.2 MHz
B_2	59 748.1 MHz	34 790.0 MHz	51 849.6 MHz	31 448.1 MHz
B_3	62 546.7 MHz	36 739.8 MHz	50 972.0 MHz	32 513.9 MHz

Table 8. CCSD(T)/aug-cc-pVTZ Dissociation Pathways of NeH_2^+ and ArH_2^+ with Energies Relative to the Respective Triatomic Cation Minima.

NeH_2^+ Products	Relative Energy	ArH_2^+ Products	Relative Energy
$\text{NeH}^+ + \text{H}$	1.031 eV	$\text{ArH}^+ + \text{H}$	0.493 eV
$\text{Ne} + \text{H}_2^+$	0.560 eV	$\text{Ar} + \text{H}_2^+$	1.838 eV
$\text{Ne}^+ + \text{H}_2$	6.503 eV	$\text{Ar}^+ + \text{H}_2$	1.930 eV
$\text{Ne} + \text{H} + \text{H}^+$	3.349 eV	$\text{Ar} + \text{H} + \text{H}^+$	4.627 eV

Table 9. The CcCR Pure Rotational Limited Line List for ArH_2^+ with $\Delta E_{J+1 \rightarrow J}, J \leq 9$ with Frequencies in MHz and Intensities in MHz (per molecule).

Molecule	J+1	J	Frequency	5000K Intensity	40K Intensity
$^{36}\text{ArH}_2^+$	1	0	122554.2	8.010×10^{-08}	0.001194
$^{36}\text{ArH}_2^+$	2	1	245087.3	3.200×10^{-07}	0.003841
$^{36}\text{ArH}_2^+$	3	2	367584.5	7.170×10^{-07}	0.006010
$^{36}\text{ArH}_2^+$	4	3	490021.7	1.270×10^{-06}	0.006426
$^{36}\text{ArH}_2^+$	5	4	612384.0	1.970×10^{-06}	0.005223
$^{36}\text{ArH}_2^+$	6	5	734650.4	2.820×10^{-06}	0.003384
$^{36}\text{ArH}_2^+$	7	6	856799.8	3.810×10^{-06}	0.001793
$^{36}\text{ArH}_2^+$	8	7	978817.3	4.930×10^{-06}	0.000789
$^{36}\text{ArH}_2^+$	9	8	1100682.0	6.180×10^{-06}	0.000291
$^{36}\text{ArH}_2^+$	10	9	1222372.7	7.540×10^{-06}	0.000091
$^{38}\text{ArH}_2^+$	1	0	122239.4	2.905×10^{-09}	0.000043
$^{38}\text{ArH}_2^+$	2	1	244457.8	1.160×10^{-08}	0.000139
$^{38}\text{ArH}_2^+$	3	2	366640.2	2.602×10^{-08}	0.000218
$^{38}\text{ArH}_2^+$	4	3	488765.6	4.606×10^{-08}	0.000234
$^{38}\text{ArH}_2^+$	5	4	610813.1	7.157×10^{-08}	0.000190
$^{38}\text{ArH}_2^+$	6	5	732767.7	1.024×10^{-07}	0.000124
$^{38}\text{ArH}_2^+$	7	6	854605.4	1.382×10^{-07}	0.000066
$^{38}\text{ArH}_2^+$	8	7	976311.1	1.789×10^{-07}	0.000029
$^{38}\text{ArH}_2^+$	9	8	1097864.0	2.241×10^{-07}	0.000011
$^{38}\text{ArH}_2^+$	10	9	1219245.9	2.735×10^{-07}	0.000003